

Creating kinks with quantum mediation

Omer Albayrak¹ and Tanmay Vachaspati^{1,2}

¹*Physics Department, Arizona State University, Tempe, Arizona 85287, USA*

²*Theoretical Physics Department, CERN, 1211 Geneva 23, Switzerland*

 (Received 21 September 2023; accepted 13 January 2024; published 1 February 2024)

We consider the creation of kink-antikink pairs of a scalar field ϕ by the scattering of classical wave packets of a second scalar field ψ when there are no direct interactions between ϕ and ψ . The creation becomes possible only due to a quantum field that interacts with both ϕ and ψ . We scan parameter space and find it favorable for kink production when the initial wave packets have large total energy and wide spatial extent but scatter at low velocities.

DOI: [10.1103/PhysRevD.109.036001](https://doi.org/10.1103/PhysRevD.109.036001)

I. INTRODUCTION

One of the most fascinating aspects of quantum field theory is the existence of nonperturbative topological structures (solitons) and their interactions with the perturbative excitations (particles) of the model [1–5]. This area of research has received much attention, but most of it has been relegated to treating the soliton sector as a fixed static or dynamical classical background. In any attempt in which solitons annihilate or are created, one is faced with the additional conceptual issue that solitons are described in terms of classical fields while particles are quantum excitations. A bridge between the soliton and particle sectors must also bridge between classical and quantum behavior, unless one can overcome the difficult problem of treating the soliton as a fully quantum object.

The creation of solitons by the scattering of particles [6–15] is of particular physical interest. Sphalerons are classical solutions in the standard model that are intermediate states in baryon-number-violating processes that are necessary to generate the cosmic matter-antimatter asymmetry [16,17]. If baryon number violation is to be experimentally tested in particle accelerators, it will be necessary to understand the creation of a sphaleron in particle collisions [18]. The expectation is that the process will be exponentially suppressed because perturbative expansions are in powers of the coupling constant, while the sphaleron and its interactions depend inversely on the coupling constant. Another process of interest is the production of magnetic monopoles in proton-proton or heavy ion scatterings such as at the Large Hadron Collider,

a process that is being searched by the MoEDAL experiment [19–21]. These searches are based on Schwinger pair production of magnetic monopoles [22,23] in relatively strong magnetic fields that can be produced as heavy ions scatter in close proximity [24–26]. The pair production rate is evaluated using instanton methods. Alternately, monopole creation by the scattering of large classical initial states of gauge bosons has been considered in Ref. [27].

While the two-particle to soliton-antisoliton process is of interest because of the way accelerators operate, one can envision situations where many particles may scatter and lead to the creation of solitons. This is the case for baryon number violation at high temperatures such as in cosmology. It may be possible that future particle machines may also involve N particle scattering where N can be large. Then the initial scattering state may be described classically, and the final state with solitons may also be adequately described using classical physics. For example, we may be interested in the production of magnetic monopoles in the scattering of intense light. The problem in this setup is that the classical description of light is given by Maxwell equations that are linear, and, classically, light does not interact with light. Colliding beams of intense light will simply pass through each other in the classical description. Only when we include quantum effects such as box diagrams does light interact with light [28–30]. Such quantum effects need occur only at intermediate stages in the scattering—the initial and final states can be described classically.

Guided by these motivations, we have studied the creation of 1 + 1-dimensional kinks in the scattering of classical initial states but those that interact with the classical kink degrees of freedom only by a quantum “bridge.” Then we have three fields: ϕ the classical field that has kink configurations, ψ the classical field that defines the initial scattering state, and ρ the quantum field that bridges between ϕ and ψ , the two classical fields.

Published by the American Physical Society under the terms of the Creative Commons Attribution 4.0 International license. Further distribution of this work must maintain attribution to the author(s) and the published article's title, journal citation, and DOI. Funded by SCOAP³.

We will set up the field theory model in more detail in Sec. II. In Sec. III, we describe the kink solution and its energy along with the initial conditions for the model. We describe the numerical method in Sec. IV and present the parameters that we have used. In Sec. V, we analyze few typical cases in detail and display the parameter space suitable for kink production. Finally, we discuss our results in Sec. VI.

II. MODEL

The Lagrangian for the model we study is

$$L = \frac{1}{2}(\partial_\mu\phi)^2 - \frac{\lambda}{4}(\phi^2 - \eta^2)^2 + \frac{1}{2}(\partial_\mu\psi)^2 - \frac{m_\psi^2}{2}\psi^2 + \frac{1}{2}(\partial_\mu\rho)^2 - \frac{1}{2}(m_\rho^2 + \alpha\phi^2 + \beta\psi^2)\rho^2, \quad (1)$$

and the equations of motion are

$$\square\phi + \lambda\phi(\phi^2 - \eta^2) + \alpha\rho^2\phi = 0, \quad (2)$$

$$\square\psi + m_\psi^2\psi + \beta\rho^2\psi = 0, \quad (3)$$

$$\square\rho + (m_\rho^2 + \alpha\phi^2 + \beta\psi^2)\rho = 0. \quad (4)$$

Ideally, all three fields should be treated in quantum field theory, but this may be unnecessary for our purposes. We will treat the incoming field ψ as a classical field. This can be justified on the grounds that our incoming state has high occupation number, typically of the order of $N \sim 10^3$. (Although high occupation number is not sufficient for a field to behave classically, we will use this criterion as a guide.) We expect quantum corrections to the initial state to be suppressed by $1/N$. The initial state evolves to excite quanta of the ρ field. Thus, the occupation number of the ρ field also grows, and parametrically it should go as $\beta^2 N$, where β is the coupling constant for the interaction between ψ and ρ . We will take $\beta = 0.5$, and so the occupation number of ρ is of the order of 10^2 . Finally, ϕ is treated classically. The occupation number for ϕ quanta is expected to be of the order of $\alpha^2(\beta^2 N)$, where α denotes the coupling between ρ and ϕ and is taken to be 0.5. This means that the occupation number of ϕ particles is also large, in the 10–100 range, and quantum corrections to the evolution of ϕ can be expected to be suppressed by $(\alpha^2\beta^2 N)^{-1} \sim 0.1$.

The key approximation enters when we include quantum backreaction on the classical background. Since ρ is a quantum operator that also appears in the ϕ and ψ classical equations of motion, we use the semiclassical approximation to write

$$\square\phi + \lambda\phi(\phi^2 - \eta^2) + \alpha\langle\rho^2\rangle\phi = 0, \quad (5)$$

$$\square\psi + m_\psi^2\psi + \beta\langle\rho^2\rangle\psi = 0, \quad (6)$$

where the expectation of ρ^2 is taken in its initial quantum state. (We work in the Heisenberg representation, in which operators evolve but the quantum states do not.) The equation for the quantum operator ρ can be solved, since the equation is linear in ρ . As discussed in Refs. [31–33], the solution is obtained using a ‘‘classical-quantum correspondence’’ (CQC) that we now summarize.

Starting with the action for the field $\rho(t, x)$,

$$\mathcal{S}_\rho = \int d^2x \left[\frac{1}{2}(\partial_\mu\rho)^2 - \frac{1}{2}(m_\rho^2 + \alpha\phi^2 + \beta\psi^2)\rho^2 \right]. \quad (7)$$

This action describes the massive quantum field ρ in the time-dependent background of $\phi(t, x)$ and $\psi(t, x)$. We continue with discretizing the action in space. On a lattice with N sites with lattice spacing a , for any field f , we define

$$f(t, x) \rightarrow f(t, ja) = f_j(t), \quad (8)$$

$$\nabla^2 f_j(t) = \frac{1}{a^2}(f_{j+1}(t) - 2f_j(t) + f_{j-1}(t)), \quad (9)$$

where $j = 1, 2, \dots, N$. The lattice under consideration is subjected to periodic boundary conditions such that, for any field $f(t, x)$, $f_{j+N}(t) = f_j(t)$. The discretized action (7) reads

$$\mathcal{S}_\rho = \int dt \frac{1}{a} \left[\frac{1}{2}\dot{\mathbf{x}}^T \dot{\mathbf{x}} - \frac{1}{2}\mathbf{x}^T \mathbf{\Omega}^2 \mathbf{x} \right], \quad (10)$$

where $\mathbf{x} = (a\rho_1, \dots, a\rho_N)^T$ and $\mathbf{\Omega}^2$ is an $N \times N$ matrix is given by

$$\Omega_{jk}^2 = \begin{cases} 2/a^2 + (m_\rho^2 + \alpha\phi_j^2 + \beta\psi_j^2) & j = k, \\ -1/a^2 & j = k \pm 1 \pmod{N}, \\ 0 & \text{otherwise.} \end{cases} \quad (11)$$

The mod N is due to the periodic boundary conditions of the lattice. The energy of the system given by the action \mathcal{S}_ρ as above can be derived as follows:

$$H_\rho = \frac{a}{2}\mathbf{p}^T \mathbf{p} + \frac{1}{2a}\mathbf{x}^T \mathbf{\Omega}^2 \mathbf{x}, \quad (12)$$

where $\mathbf{p} = \dot{\mathbf{x}}/a$. This expression is precisely the Hamiltonian of N coupled harmonic oscillators with a time-dependent spring constant matrix.

The Hamiltonian in (12) can be mapped to a classical system. The technique is to use the Bogoliubov transformations to map the N coupled quantum harmonic oscillator problem to an N^2 classical harmonic oscillator problem whose variables are written as an $N \times N$ matrix

$\mathbf{Z}(t) = [Z_{jk}(t)]$ and the corresponding momentum matrix $\mathbf{P}(t) = [P_{jk}(t)] = \dot{\mathbf{Z}}/a$ [33]. The mapping is given by

$$\mathbf{x} = \mathbf{Z}^* \mathbf{a}_0 + \mathbf{Z} \mathbf{a}_0^{\dagger T}, \quad (13)$$

$$\mathbf{p} = \mathbf{P}^* \mathbf{a}_0 + \mathbf{P} \mathbf{a}_0^{\dagger T}, \quad (14)$$

where $\mathbf{a} = (a_1, \dots, a_N)^T$ and $\mathbf{a}^\dagger = (a_1^\dagger, \dots, a_N^\dagger)$ are the ladder operators for each of the N harmonic oscillators and the subscript “0” represents the operators at the initial time t_0 . The quantum field $\rho(x, t)$ can now be represented in terms of corresponding expressions of \mathbf{Z} and \mathbf{P} (or, equivalently, $\dot{\mathbf{Z}}$) using (13) and (14).

The resulting classical system of $\mathbf{Z}(t)$ has the following action:

$$\mathcal{S}_c = \int dt \frac{1}{2a} \text{Tr}[\dot{\mathbf{Z}}^\dagger \dot{\mathbf{Z}} - \mathbf{Z}^\dagger \Omega^2 \mathbf{Z}], \quad (15)$$

and the equations of motion are

$$\mathbf{Z} + \Omega^2 \mathbf{Z} = 0, \quad (16)$$

which are to be solved with the initial conditions

$$\mathbf{Z}_0 = -i\sqrt{\frac{a}{2}}\sqrt{\Omega}^{-1} \quad \text{and} \quad \dot{\mathbf{Z}}_0 = \sqrt{\frac{a}{2}}\sqrt{\Omega}. \quad (17)$$

Since the CQC provides an exact correspondence of the quantum problem into its classical counterpart, from now on we need only Eq. (16) and initial conditions (17) to fully understand the time evolution of the quantum field. The quantum evolution of ρ is then obtained from (13) and (14).

The vacuum expectation value of ρ^2 at the spatial point labeled by i can be written in terms of \mathbf{Z} as

$$\langle \rho_i^2 \rangle = \frac{1}{a^2} \sum_{j=1}^N Z_{ij}^* Z_{ij} \quad (18)$$

using (13). Therefore, from (5) and (6), the discretized equations we would like to solve for ϕ and ψ are

$$\ddot{\phi}_i - \nabla^2 \phi_i + \lambda \phi_i (\phi_i^2 - \eta^2) + \frac{\alpha}{a^2} \sum_{j=1}^N Z_{ij}^* Z_{ij} \phi_i = 0, \quad (19)$$

$$\ddot{\psi}_i - \nabla^2 \psi_i + m_\psi^2 \psi_i + \frac{\beta}{a^2} \sum_{j=1}^N Z_{ij}^* Z_{ij} \psi_i = 0, \quad (20)$$

where we use second-order spatial differences as in (9) to calculate the Laplacians. The equation for Z_{ij} is

$$\ddot{Z}_{ij} + \Omega_{ik}^2 Z_{kj} = 0. \quad (21)$$

The system of equations (19)–(21) need to be solved with suitable boundary conditions that we will discuss below. Before proceeding to the solution, however, the issue of renormalization needs to be addressed.

The parameters appearing in the above equations of motion are bare parameters that will get dressed by quantum effects. This can also be seen by realizing that the quantity $\langle \rho_i^2 \rangle$ in (18) diverges as $\log(N)$ as $N \rightarrow \infty$. The divergence can be absorbed in the mass parameters m_ϕ and m_ψ [34,35]. Equivalently, we can subtract out the fluctuations in the trivial vacuum:

$$\langle \rho_i^2 \rangle \rightarrow \langle \rho_i^2 \rangle - \langle \rho_i^2 \rangle_0, \quad (22)$$

where

$$\langle \rho_i^2 \rangle_0 \equiv \frac{1}{a^2} \sum_{j=1}^N Z_{ij}^* Z_{ij} \Big|_0. \quad (23)$$

The “0” subscript refers to the trivial vacuum with $\phi = \eta$ and $\psi = 0$.

The energy in the quantum field ρ can now be written as

$$E_\rho = \frac{1}{2a} \text{Tr}[\dot{\mathbf{Z}}^\dagger \dot{\mathbf{Z}} + \mathbf{Z}^\dagger \Omega^2 \mathbf{Z}], \quad (24)$$

and the discrete energy density

$$\epsilon_{\rho,i} = \frac{1}{a^2} \sum_k \left\{ \frac{1}{2} |\dot{Z}_{ij}|^2 + \frac{1}{4a^2} [|Z_{i+1j} - Z_{ij}|^2 + |Z_{ij} - Z_{i-1j}|^2] + \frac{1}{2} [m_\rho^2 + \alpha \phi_j^2 + \beta \psi_j^2] |Z_{ij}|^2 \right\}. \quad (25)$$

Owing to the last term, this expression also suffers from the divergence mentioned above. We use the same renormalizing scheme to remove the lattice dependence and to obtain a finite expression even as $N \rightarrow \infty$:

$$\epsilon_{\rho,i}^R = \epsilon_{\rho,i} - \frac{1}{2} [m_\rho^2 + \alpha \phi_i^2 + \beta \psi_i^2] \langle \hat{\rho}_i^2 \rangle_0 - \epsilon_{\rho,i} |_0, \quad (26)$$

where the last term is added for the purpose of subtracting out the zero-point energy. The total energy of ρ is similarly defined:

$$E_\rho^R = E_\rho - \frac{1}{2} \sum_{i=1}^N [m_\rho^2 + \alpha \phi_i^2 + \beta \psi_i^2] \langle \hat{\rho}_i^2 \rangle_0 - E_\rho |_0. \quad (27)$$

By adding the energy of the fields ϕ and ψ , the total conserved energy of the system is

$$E = E_{\phi+\psi} + E_\rho^R, \quad (28)$$

where $E_{\phi+\psi}$ is defined as

$$E_{\phi+\psi} = \sum_i \left\{ \frac{1}{2} [\dot{\phi}_i^2 + \phi_i'^2 + \dot{\psi}_i^2 + \psi_i'^2] + \frac{1}{2} m_\psi^2 \psi_i^2 + \frac{\lambda}{4} (\phi_i^2 - \eta^2)^2 \right\}. \quad (29)$$

Spatial first derivatives are calculated using central differencing:

$$f'_i = \frac{f_{i+1} - f_{i-1}}{2a}. \quad (30)$$

To summarize this section, the final equations we wish to solve are

$$\begin{aligned} \ddot{\phi}_i - \nabla^2 \phi_i + \lambda \phi_i (\phi_i^2 - \eta^2) \\ + \frac{\alpha}{a^2} \sum_{j=1}^N (Z_{ij}^* Z_{ij} - Z_{ij}^* Z_{ij}|_0) \phi_i = 0, \end{aligned} \quad (31)$$

$$\begin{aligned} \ddot{\psi}_i - \nabla^2 \psi_i + m_\psi^2 \psi_i \\ + \frac{\beta}{a^2} \sum_{j=1}^N (Z_{ij}^* Z_{ij} - Z_{ij}^* Z_{ij}|_0) \psi_i = 0 \end{aligned} \quad (32)$$

and also Eq. (21) for \mathbf{Z} .

III. INITIAL CONDITIONS

We are interested in the creation of Z_2 kinks of ϕ due to collisions of classical wave packets of ψ . The kink configurations are solutions of the model

$$L_\phi = \frac{1}{2} (\partial_\mu \phi)^2 - \frac{\lambda}{4} (\phi^2 - \eta^2)^2, \quad (33)$$

and boosted kinks are given by the solutions

$$\phi_K(t, x) = \pm \eta \tanh \left(\sqrt{\frac{\lambda}{2}} \eta \gamma (x - vt) \right), \quad (34)$$

where the Lorentz boost factor $\gamma = 1/\sqrt{1-v^2}$, the + sign denotes a kink, and a - sign denotes an antikink. The energy of the kink (or antikink) is given by

$$E_K = \gamma \frac{2\sqrt{2}}{3} \sqrt{\lambda} \eta^3. \quad (35)$$

In the classical scattering of ψ , kinks cannot be created without the participation of the quantum field ρ , because ϕ and ψ have no direct coupling. Initially, there are no kinks, and we take ϕ to be in its vacuum state:

$$\phi(t=0, x) = \eta, \quad \dot{\phi}(t=0, x) = 0. \quad (36)$$

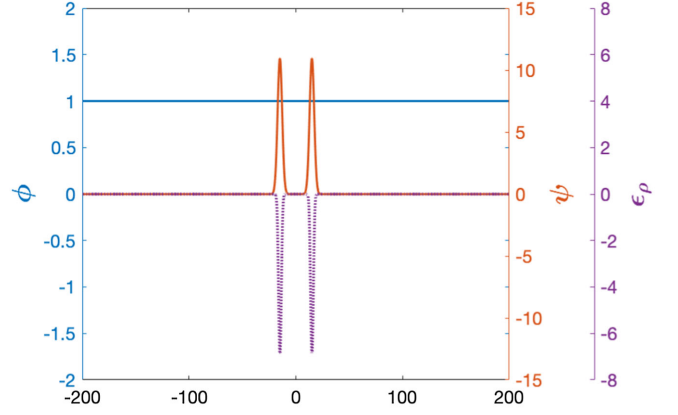


FIG. 1. Initial field configurations for ϕ (blue line) and ψ (orange line) and initial renormalized energy density of ρ (dashed purple line).

Our choice for the initial conditions for ψ contains two Gaussian wave packets that move toward each other with velocity v . Then,

$$\psi(t=0, x) = F(\gamma(x+x_0)) + F(\gamma(x-x_0)), \quad (37)$$

where $\gamma = 1/\sqrt{1-v^2}$, $2x_0$ is the initial ($t=0$) wave packet separation, and

$$F(x) = A e^{-kx^2}. \quad (38)$$

We also have

$$\dot{\psi}(t=0, x) = \gamma v [F'(\gamma(x+x_0)) - F'(\gamma(x-x_0))], \quad (39)$$

where primes denote derivatives with respect to the argument.

The quantum field ρ is initially assumed to be in its ground state in the background of $\phi(t=0, x)$ and $\psi(t=0, x)$. In terms of \mathbf{Z} , this is given by Eq. (17), where the matrix $\mathbf{\Omega}_0^2$ is evaluated from (11) using the initial values of ϕ and ψ .

In Fig. 1, we show the ϕ and ψ fields and the renormalized energy density in ρ at the initial time.

IV. NUMERICAL METHOD

There are a large number of parameters that we need to fix before we can solve the equations. We choose

$$\begin{aligned} \lambda = 1, \quad \eta = 1, \quad \alpha = 0.5, \quad m_\rho = 1, \\ m_\psi = 1, \quad \beta = 0.5. \end{aligned} \quad (40)$$

The equations of motion are evolved using the position Verlet method with lattice spacing $a = 0.4$ and time step $dt = a/50$ on a periodic lattice with $N = 1000$. The code is evolved for less than a light-crossing time to prevent

interference from excitations that propagate all the way across the lattice.

There are also several parameters associated with the initial conditions: x_0 , A , v , and k . The initial separation of the Gaussian wave packets is fixed to be $2x_0 = 30$. This is large enough that the overlap of the Gaussian wave packets is minimal for all runs. We scan over A , v , and k in the following intervals:

$$A \in [7, 16], \quad v \in [0.1, 0.8], \quad k = 0.03, 0.1, 0.3. \quad (41)$$

There is some ambiguity in deciding if the scattering has led to kink-antikink production. The simplest definition is to identify a zero of ϕ as a kink or an antikink (depending on the gradient of ϕ at the location of the zero). However, two zeros representing a kink and an antikink may be very close to each other, and they may eventually annihilate. A further refinement of the criterion that we adopt is to require that the distance between zeros be larger than 4 times the kink width and should increase with time.

V. RESULTS

In this section, we present our simulation results based on the methods mentioned above. Initially, we analyze a few distinct cases as examples for kink creation. Subsequently, we study the regions within parameter space that satisfy the conditions necessary for kink formation.

In Fig. 2, we illustrate a clear case of kink production. The three snapshots of the evolution for $v = 0.3$ and $A = 11.0$ show the collision of the ψ wave packets and the creation of a kink-antikink pair that separates out with velocities ± 0.68 , respectively. Initially, there is some energy in ρ that propagates together with the incoming wave packets. After the collision, if kinks are created, they too carry some ρ energy along with them. In addition, we observe that there is energy in ρ not directly related to the interactions with the initial Gaussian wave packets or the

final kinks. This energy is in the form of quantum radiation and can be seen in Fig. 3(a). The evolution of the total energy in the various fields is shown in Fig. 3(b).

From Fig. 3(b), we see that the initial energy is ~ 500 in units of $\sqrt{\lambda}$, whereas the energy of a kink ~ 1 from (35) and that of a kink-antikink pair is ~ 2 . The collision has, therefore, converted less than a percent of the initial energy into solitons; the rest is in radiative modes.

With somewhat different parameters, the evolution can be quite different, with the production of several kink-antikink pairs. An example is shown in Fig. 4 for the parameters $v = 0.25$ and $A = 13.5$. Now the evolution leads to a lot more fluctuations of ϕ , and there are many zeros of ϕ at the final time. With further evolution, we expect some of the zeros to annihilate, but by our criteria, described in Sec. IV, this final state contains five kink-antikink pairs. Now the energy density in ρ is more spread out as in Fig. 5(a), and the total energies in the fields show an interesting crossover in Fig. 5(b), where most of the energy ends up in the quantum field ρ .

In this case, we start out with a higher initial energy ~ 750 , but we end up with five kink-antikink pairs with energy ~ 10 which is a higher fraction of the initial energy than in the case of Fig. 2. However, it is not clear how many of the five kink-antikink pairs will survive at very late times. The complexity is shown in Fig. 6, where we plot the zeros of ϕ as a function of time. In the case of Fig. 2, the zeros are shown in Fig. 6(a), there is only one kink-antikink pair, and they are separating with velocity $\sim \pm 0.68$. In the case corresponding to Fig. 4, the plot of zeros of ϕ is shown in Fig. 6(b). The outermost zeros are moving apart with $\sim \pm 0.78$, but the inner ones are slower and some annihilations are very likely.

In order to find initial conditions that are favorable for the production of kinks, we have evolved the system for the range of initial conditions given in (41) and checked which initial conditions lead to kink production. Our results are shown in Fig. 7 and indicate favorable conditions for kink

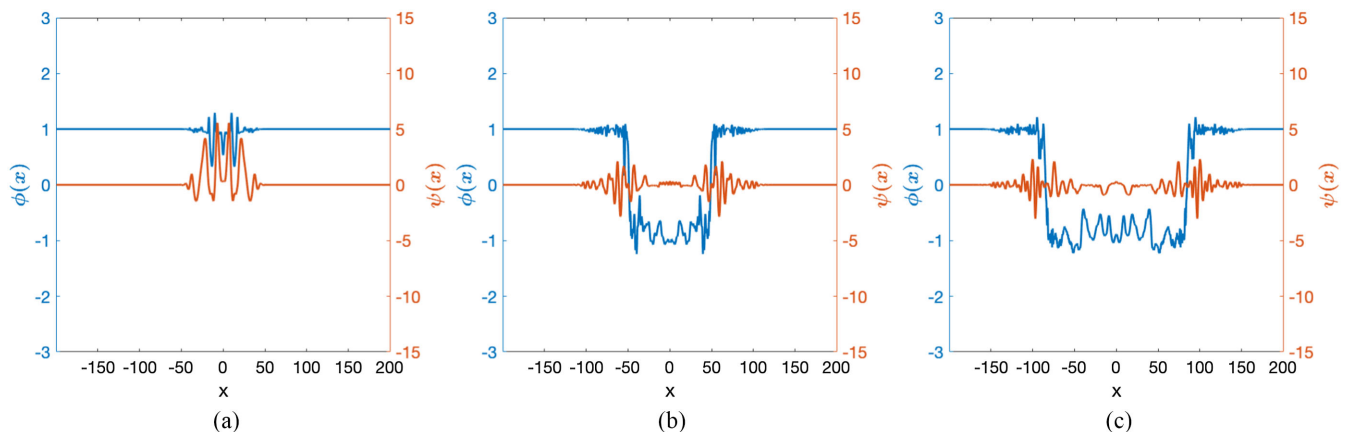


FIG. 2. Three snapshots of the time evolution of the fields ϕ and ψ with initial parameters $v = 0.3$ and $A = 11.0$. This is a clear case where a kink-antikink pair is produced.

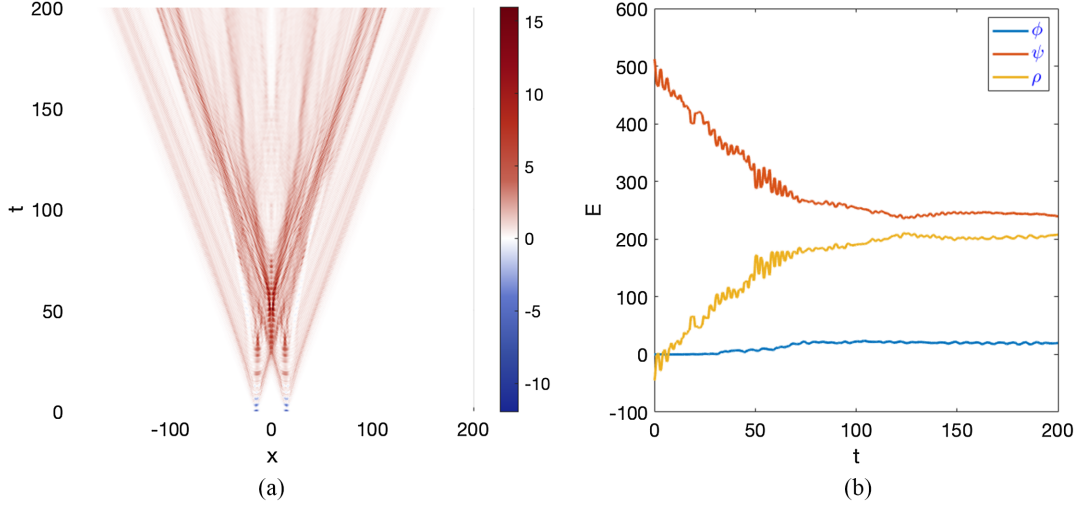


FIG. 3. (a) Evolution of the energy density $\epsilon_{\rho,i}$ for $v = 0.3$ and $A = 11.0$. At the initial time, the quantum fluctuations are affected by the wave packets of ψ , and there is nonvanishing energy density of ρ within the wave packets. Once kinks are created ($t \gtrsim 50$), energy in the quantum fluctuations of ρ is carried by the kink-antikink pair. In addition, ρ particles are radiated. (b) Total energies of the individual fields over time. For ϕ and ψ , only their kinetic, gradient, and potential terms are included [see (29)]. The suitably renormalized interaction energy is included in ρ . The final energy in the kink field, ϕ , is $E_{\phi,\text{final}} \sim 21.02$, which is about 10 times the energy in the kink-antikink pair.

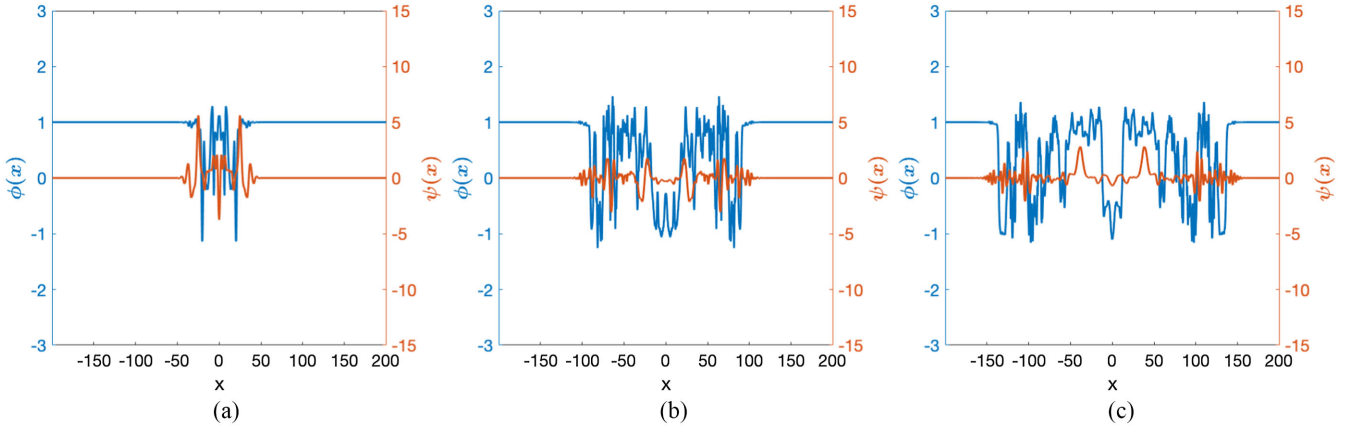


FIG. 4. Three snapshots of the time evolution of the fields ϕ and ψ with initial parameters $v = 0.25$ and $A = 13.5$. We observe a somewhat chaotic behavior where there are multiple kink-antikink creations.

production for large A and small v (at least in the $k = 0.1, 0.3$ cases). However, the results suggest a fractal structure, and there are lots of holes in the parameter space where otherwise one may expect kink production. There are also isolated special places in parameter space where a large number of kinks are produced.

From Fig. 7, it is clear that choosing wider Gaussian wave packets (smaller k) is more favorable to kink production. A first thought is that smaller k might imply higher initial energy, which would explain the greater rate of kink production, but that is not necessarily the case, since the initial energy in ψ can be calculated explicitly in the limit of large x_0 by using (37) and (39) in (29) (see the Appendix):

$$E_{\psi}(t=0) = \sqrt{\frac{\pi}{2}} \gamma A^2 \left[(1+v^2)\sqrt{k} + \frac{m_{\psi}^2}{\sqrt{k}}(1-v^2) \right]. \quad (42)$$

For fixed v , $E_{\psi}(t=0)$ is minimum when

$$k = k_* = m_{\psi}^2 \left(\frac{1-v^2}{1+v^2} \right), \quad (43)$$

and the energy does not monotonically increase with decreasing k . While it is true that, for our choice of values of k and v in (41), the initial energy is higher for smaller values of k , the energies for $k = 0.1$ and $k = 0.3$ and with $v = 0.8$ are very close, to within 6%, yet there is much

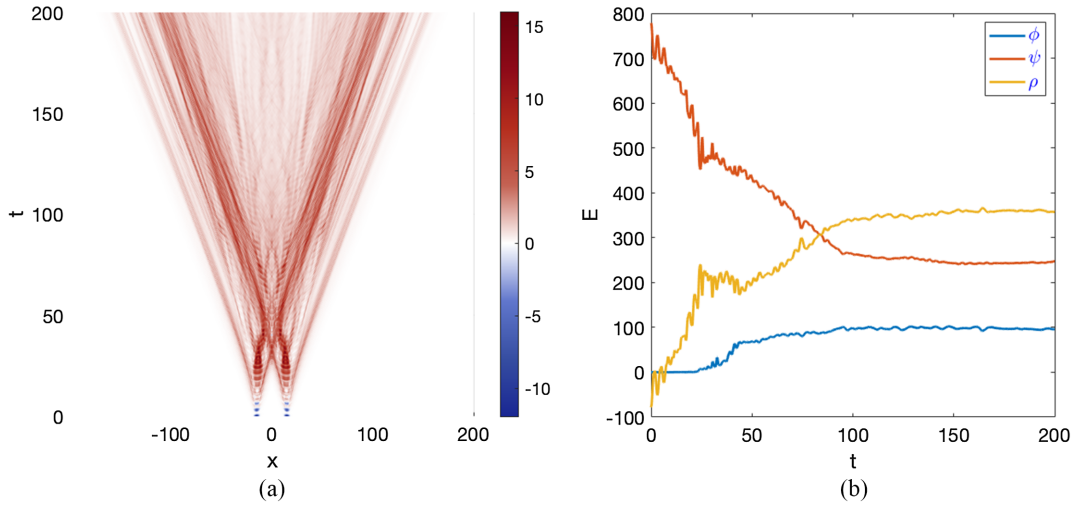


FIG. 5. (a) Space-time plot of energy density $\epsilon_{\rho,i}$. Imprints of the initial ψ wave packets and resulting kink-antikinks in ϕ are observed. (b) Energies of individual fields over time. For ϕ and ψ , only kinetic, gradient, and potential terms are included. Interaction energy is included in ρ with apt renormalization. $E_{\phi,\text{final}} \sim 101.8E_K|_{\gamma=1}$. The parameters are $v = 0.25$ and $A = 13.5$.

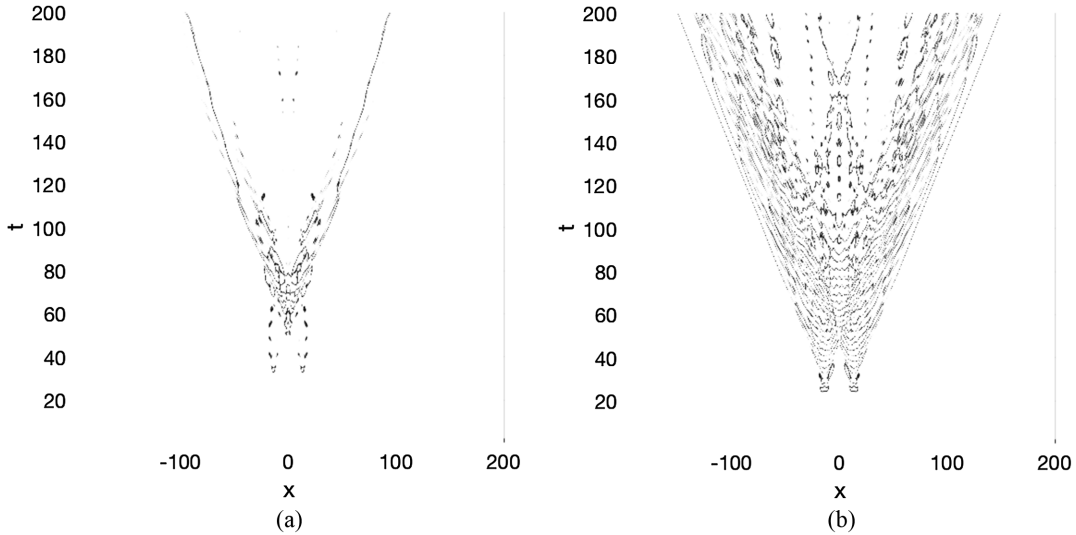


FIG. 6. The space-time graphs of zeros of ϕ for cases (a) $v = 0.3$, $A = 11.0$ and (b) $v = 0.25$, $A = 13.5$. Only zeros that are well separated (four kink widths) and moving away with time from their neighbors are counted as kink-antikinks. These plots also display the kink-antikink pairs that are created but annihilate during the simulation.

more kink production with $k = 0.03$ than with $k = 0.1$. This suggests that a more spread out wave packet in the initial conditions is favorable for kink production.

To explore the effect of changing Gaussian width and wave packet velocity, we have performed several runs in which the total initial energy in ψ is fixed. We implement this by choosing

$$A^2 = \frac{E_i}{\sqrt{\frac{2}{\gamma}}[(1+v^2)\sqrt{k} + \frac{m_\psi^2}{\sqrt{k}}(1-v^2)]} \quad (44)$$

for some choice of initial energy E_i . We scan over parameters k and v , adjusting A^2 according to (44) so that

the initial energy stays fixed (up to very tiny corrections due to the quantum fluctuations of ρ and exponentially small corrections due to the overlap of the two wave packets). The results are shown in Fig. 8 for fixed initial energy of 250, 400, and 550. The first feature that stands out is that for fixed $E_{\psi,0} = 250$ there is only a very small area that yields kink production as seen in Fig. 8(a), which suggests an energy threshold for kink production for the model. Figures 8(b) and 8(c) exhibit similar band patterns, although the location and size of these bands are slightly different; for example, the gap between the two bright bands is larger for $E_{\psi,0} = 400$. The plots show the general trend that higher energy, wider wave packets, and slower

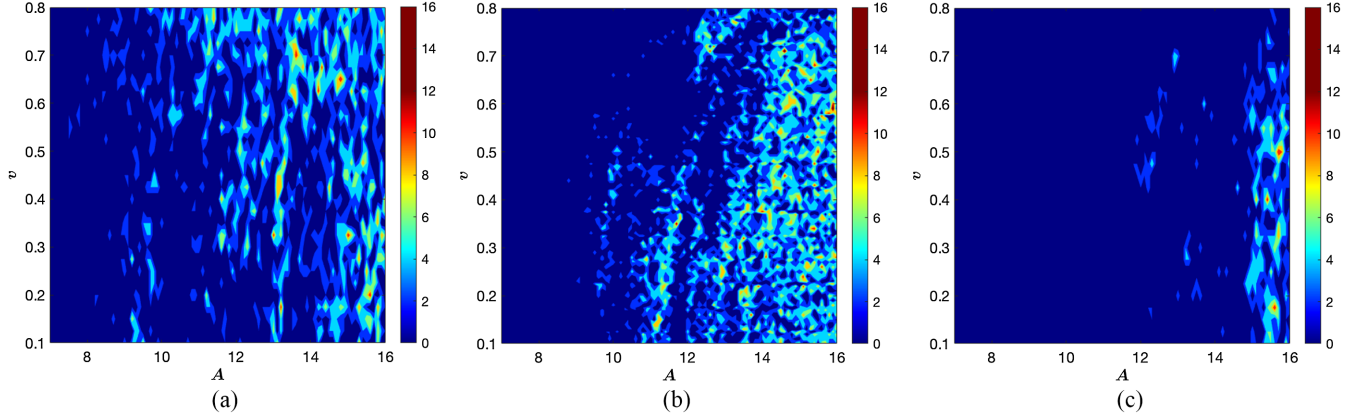


FIG. 7. Kink-antikink pair production in the amplitude (A) and velocity (v) plane as a contour plot for (a) $k = 0.03$, (b) $k = 0.1$, and (c) $k = 0.3$. The color bar shows the total number of kink-antikinks produced—a kink-antikink pair counts as 2 on the color bar. The gaps are genuine and show chaotic behavior—simply increasing the amplitude, for example, does not guarantee kink production. Since the width of the initial wave packets decreases as k increases, the plots show that kink production is favored for larger widths.

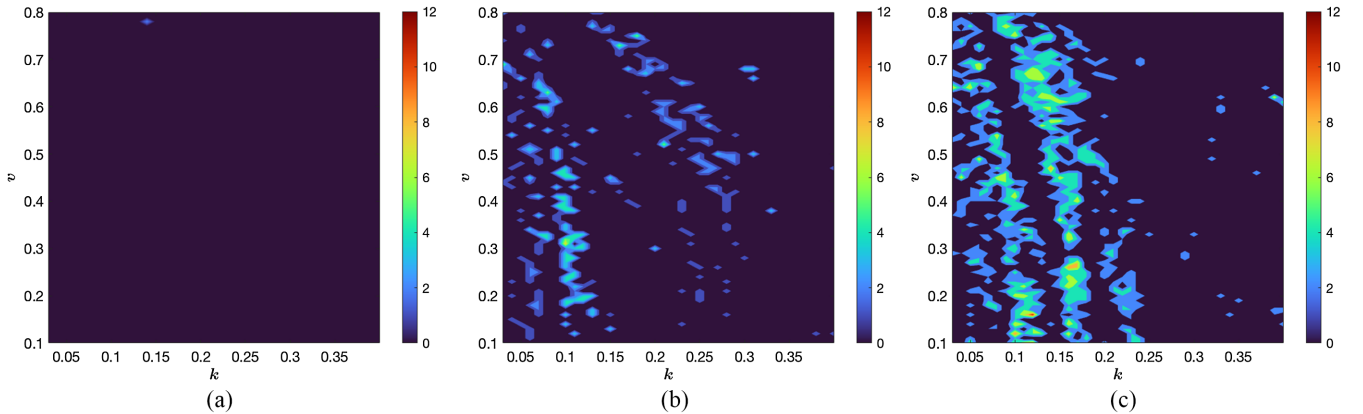


FIG. 8. Kink-antikink pair production at fixed initial energies (a) $E_{\psi,0} = 250$, (b) $E_{\psi,0} = 400$, and (c) $E_{\psi,0} = 550$ showing enhanced production at small k (wider wave packets) scattering at low velocities. In (a), there is only one case of kink production at $k = 0.14$ and $v = 0.78$.

scattering velocities create favorable conditions for kink production.

VI. CONCLUSIONS

We have studied the creation of classical kinks by scattering classical wave packets but where the wave packet and kink interactions are mediated by a quantum field. This setup was motivated by the case of monopole production in light on light scattering, since classical light on light scattering is trivial and becomes nontrivial only when quantum effects, such as box diagrams, are included. However, there are differences between our toy model and the physical case of magnetic monopole production. In the latter, light on light scattering would produce heavy gauge bosons due to quantum interactions, and the heavy gauge bosons themselves would form the magnetic

monopoles. This is unlike in our toy model, where we have chosen a classical field, distinct from the quantum fields, that composes the kinks. Our choice was necessary, because kinks are conveniently described as classical configurations, not as a conglomerate of quantum particles.

We have scanned a set of parametrized initial conditions for successful kink production. Certain trends are clear within our analysis. The initial conditions that led to kink production in our simulations all have total energy that is 10^2 – 10^3 times the energy in a kink-antikink pair. However, the energy per quanta need not be large and is of the order of m_ψ as the velocities are only mildly relativistic. In fact, we found that it is somewhat favorable to choose moderate velocities, $v \sim 0.5$, but to have large values of the amplitude A corresponding to a large number of quanta in the initial state, $N \sim E/m_\psi \sim 10^2$ – 10^3 . There is no systematic trend, however, and there are “holes” in our scan of parameter

space as seen in Fig. 7. This suggests that there may be resonances at work—if certain frequencies match, kink production is more favorable. It would be of interest to find initial conditions with less energy and that convert into kink-antikink pairs more efficiently.

We have investigated the effect of the width of the initial wave packets and the scattering velocity on the kink production with fixed initial energies. It is clear from Fig. 8 that there is a lower energy threshold and wider wave packets with lower velocities provide better conditions for kink production. We also observe a band structure where certain widths seems more favorable than others. It is also worth noting that production is significantly lower for smaller widths (higher k) in all the cases.

Our analysis is of an exploratory nature, as magnetic monopole production in the real world is much more complicated. Yet our analysis suggests that scattering at high luminosities is much more desirable than scattering at high energies if the goal is to produce magnetic monopoles.

ACKNOWLEDGMENTS

We thank Mainak Mukhopadhyay and George Zahariade for useful comments. T. V. is grateful to the University of Geneva for hospitality while this work was being done. This work was supported by the U.S. Department of Energy, Office of High Energy Physics, under Grant No. DE-SC0019470.

APPENDIX: ENERGY OF THE INITIAL WAVE PACKETS

We ignore the quantum corrections to the energy of the initial wave packets as these are small [see Figs. 3(b)

and 5(b)] and consider widely separated wave packets in which case the initial energy is just twice that of a single wave packet:

$$E_{\psi,0} = 2 \int dx \left[\frac{1}{2} (\dot{\psi}^2 + \psi'^2) + \frac{m_{\psi}^2}{2} \psi^2 \right] \quad (\text{A1})$$

with

$$\psi = Ae^{-kX^2}, \quad \dot{\psi} = \gamma v A (-2kX) e^{-kX^2}, \quad (\text{A2})$$

where $X = \gamma(x + x_0)$. This leaves us with Gaussian integrals, and we get

$$E_{\psi}(t=0) = \sqrt{\frac{\pi}{2}} \gamma A^2 \left[(1 + v^2) \sqrt{k} + \frac{m_{\psi}^2}{\sqrt{k}} (1 - v^2) \right]. \quad (\text{A3})$$

This expression can also be written as

$$E_{\psi}(t=0) = \gamma E_{\psi,v=0} + \sqrt{\frac{\pi}{2}} \gamma v^2 A^2 \left[\sqrt{k} - \frac{m_{\psi}^2}{\sqrt{k}} \right]. \quad (\text{A4})$$

Note that $E_{\psi}(t=0)$ is not $\gamma E_{\psi,v=0}$ as we might expect from special relativistic boosts. This is because the Gaussian wave packet is not a solution of the static equations of motion. Only static solutions of the equations of motion obey the special relativistic transformation when boosted.

For $k < m_{\psi}^2$, the term in square brackets in (A4) can be negative, and it may happen that the initial energy *decreases* with increasing v .

-
- [1] *Solitons and Particles*, edited by C. Rebbi and G. Soliani (World Scientific, Singapore, 1985).
 - [2] R. Rajaraman, *Solitons and Instantons. An Introduction to Solitons and Instantons in Quantum Field Theory* (North-Holland, Amsterdam, 1982).
 - [3] T. Vachaspati, *Kinks and Domain Walls: An Introduction to Classical and Quantum Solitons* (Oxford University Press, New York, 2007).
 - [4] N. S. Manton and P. Sutcliffe, *Topological Solitons*, Cambridge Monographs on Mathematical Physics (Cambridge University Press, Cambridge, England, 2004).
 - [5] A. Vilenkin and E. P. S. Shellard, *Cosmic Strings and Other Topological Defects* (Cambridge University Press, Cambridge, England, 2000).
 - [6] A. K. Drukker and S. Nussinov, Monopole pair creation in energetic collisions: Is it possible?, *Phys. Rev. Lett.* **49**, 102 (1982).
 - [7] D. G. Levkov and S. M. Sibiryakov, Induced tunneling in quantum field theory: Soliton creation in collisions of highly energetic particles, *Phys. Rev. D* **71**, 025001 (2005).
 - [8] T. Romanczukiewicz, Creation of kink and antikink pairs forced by radiation, *J. Phys. A* **39**, 3479 (2006).
 - [9] S. Dutta, D. A. Steer, and T. Vachaspati, Creating kinks from particles, *Phys. Rev. Lett.* **101**, 121601 (2008).
 - [10] T. Romanczukiewicz and Y. Shnir, Oscillon resonances and creation of kinks in particle collisions, *Phys. Rev. Lett.* **105**, 081601 (2010).
 - [11] S. V. Demidov and D. G. Levkov, Soliton-antisoliton pair production in particle collisions, *Phys. Rev. Lett.* **107**, 071601 (2011).
 - [12] S. V. Demidov and D. G. Levkov, Soliton pair creation in classical wave scattering, *J. High Energy Phys.* **06**(2011)016.
 - [13] H. Lamm and T. Vachaspati, Numerical exploration of soliton creation, *Phys. Rev. D* **87**, 065018 (2013).

- [14] P. Dorey, A. Halavanau, J. Mercer, T. Romanczukiewicz, and Y. Shnir, Boundary scattering in the ϕ^4 model, *J. High Energy Phys.* **05** (2017) 107.
- [15] S. V. Demidov and D. G. Levkov, Semiclassical description of soliton-antisoliton pair production in particle collisions, *J. High Energy Phys.* **11** (2015) 066.
- [16] F. R. Klinkhamer and N. S. Manton, A saddle-point solution in the Weinberg-Salam theory, *Phys. Rev. D* **30**, 2212 (1984).
- [17] D. E. Morrissey and M. J. Ramsey-Musolf, Electroweak baryogenesis, *New J. Phys.* **14**, 125003 (2012).
- [18] A. Papaefstathiou, S. Plätzer, and K. Sakurai, On the phenomenology of sphaleron-induced processes at the LHC and beyond, *J. High Energy Phys.* **12** (2019) 017.
- [19] B. Acharya *et al.* (MoEDAL Collaboration), The physics programme of the MoEDAL experiment at the LHC, *Int. J. Mod. Phys. A* **29**, 1430050 (2014).
- [20] B. Acharya *et al.* (MoEDAL Collaboration), Search for magnetic monopoles with the MoEDAL forward trapping detector in 13 TeV proton-proton collisions at the LHC, *Phys. Rev. Lett.* **118**, 061801 (2017).
- [21] V. A. Mitsou (MoEDAL Collaboration), First search for magnetic monopoles through the Schwinger mechanism, *J. Phys. Conf. Ser.* **2375**, 012002 (2022).
- [22] I. K. Affleck and N. S. Manton, Monopole pair production in a magnetic field, *Nucl. Phys.* **B194**, 38 (1982).
- [23] I. K. Affleck, O. Alvarez, and N. S. Manton, Pair production at strong coupling in weak external fields, *Nucl. Phys.* **B197**, 509 (1982).
- [24] D. L. J. Ho and A. Rajantie, Classical production of 't Hooft-Polyakov monopoles from magnetic fields, *Phys. Rev. D* **101**, 055003 (2020).
- [25] A. Rajantie, Monopole-antimonopole pair production by magnetic fields, *Phil. Trans. R. Soc. A* **377**, 20190333 (2019).
- [26] D. L. J. Ho and A. Rajantie, Instanton solution for Schwinger production of 't Hooft-Polyakov monopoles, *Phys. Rev. D* **103**, 115033 (2021).
- [27] T. Vachaspati, Creation of magnetic monopoles in classical scattering, *Phys. Rev. Lett.* **117**, 181601 (2016).
- [28] O. Halpern, Scattering processes produced by electrons in negative energy states, *Phys. Rev.* **44**, 855 (1933).
- [29] G. Breit and J. A. Wheeler, Collision of two light quanta, *Phys. Rev.* **46**, 1087 (1934).
- [30] H. Euler and B. Kockel, The scattering of light by light in Dirac's theory, *Naturwissenschaften* **23**, 246 (1935).
- [31] T. Vachaspati and G. Zahariade, Classical-quantum correspondence and Hawking radiation, *J. High Energy Phys.* **04** (2019) 013.
- [32] T. Vachaspati and G. Zahariade, Classical-quantum correspondence and backreaction, *Phys. Rev. D* **98**, 065002 (2018).
- [33] T. Vachaspati and G. Zahariade, Classical-quantum correspondence for fields, *J. High Energy Phys.* **09** (2019) 015.
- [34] M. Mukhopadhyay, E. I. Sfakianakis, T. Vachaspati, and G. Zahariade, Kink-antikink scattering in a quantum vacuum, *J. High Energy Phys.* **04** (2022) 118.
- [35] M. Mukhopadhyay and T. Vachaspati, Resonance structures in kink-antikink scattering in a quantum vacuum, *Phys. Rev. D* **107**, 116017 (2023).